



BaFe₁₂O₁₉ powder with high magnetization prepared by acetone-aided coprecipitation

Hsuan-Fu Yu *

Department of Chemical and Materials Engineering, Ceramic Materials Laboratory, Tamkang University, New Taipei City 25137, Taiwan

ARTICLE INFO

Article history:

Received 2 December 2012

Received in revised form

26 March 2013

Available online 16 April 2013

Keywords:

Barium hexaferrite

Coprecipitation

Magnetic property

Magnetization

Hard magnets

ABSTRACT

BaFe₁₂O₁₉ particles with high magnetization were produced using an acetone-aided coprecipitation process. An aqueous solution of iron and barium nitrates, in an Fe³⁺/Ba²⁺ molar ratio of 12, was added in a stirred precipitation liquid medium composed of H₂O, CH₃(CO)CH₃ and NH₄OH. After reacting metallic ions with ammonia, the precipitates were formed, centrifugally filtered, freeze dried and calcined. Effects of amount of the acetone in the precipitation liquid medium on the formation of crystalline BaFe₁₂O₁₉ were investigated. The presence of acetone in the precipitation liquid medium can greatly promote formation of the crystalline BaFe₁₂O₁₉ at temperature as low as 650 °C and can enhance magnetization of the derived particles. On the other hand, raising the calcination temperature can effectively accelerate development of crystallite morphology and magnetic characters of the barium hexaferrites. While the barium hexaferrite powder obtained without acetone additions and calcined at 1000 °C had magnetization (measured at 50 kOe; *M*(50 kOe)) of 63.5 emu/g, remanence magnetization (*Mr*) of 31.3 emu/g and coercivity (*Hc*) of 4.7 kOe, the single magnetic domain size BaFe₁₂O₁₉ powder with *M*(50 kOe) of 70.6 emu/g, *Mr* of 34.4 emu/g and *Hc* of 3.7 kOe was produced at 1000 °C, using a precipitation liquid medium of 64 vol% acetone.

© 2013 Elsevier B.V. All rights reserved.

1. Introduction

Barium hexaferrite (BaFe₁₂O₁₉), as permanent magnet, is widely used in electronic industries due to its excellent magnetic properties, such as large magnetization (72 emu/g at 25 °C), high Curie temperature (450 °C), high magnetic anisotropy and high coercivity (6.7 kOe), as well as excellent chemical stability and corrosion resistivity [1–6]. The characteristics of BaFe₁₂O₁₉ particles are very important for manufacturing permanent ceramic magnets because of their influence on the quality of final products. To have a better performance, barium hexaferrite particles are required to be of single magnetic domain, good chemical homogeneity and narrow particle size distribution. Conventionally, solid-state reactions (or call ceramic methods), including milling and firing of the mixture of iron oxide and barium carbonate, are used to synthesize barium hexaferrite powder. The firing temperatures used are 1200 °C or above [7,8]. Although firing at high temperatures assures the formation of BaFe₁₂O₁₉ phase, larger particles (> 1 μm) are often obtained in this firing stage. Milling the solids usually leads to introduction of impurities into material compositions, generation of lattice strains in molecular structure and production of particles

with irregular shape. All of these will have negative impacts on developing microstructures of the ferrite products. Therefore, several nonconventional techniques, such as the glass crystallization method [9–12], the hydrothermal technique [13–17], the precursor method [18–22], the coprecipitation method [23–27] and others, have been used or are under development for preparing ultrafine barium hexaferrite particles. Among these, the coprecipitation method is one of the techniques suitable for the low-cost and mass production of barium hexaferrite particles.

In coprecipitation, the salts containing iron and barium elements are dissolved in a proper solvent to form a solution, followed by adding the precipitating agent to force the metallic cations in the solution to convert to solid phase(s), as precipitates. The solid precipitates were then calcined at predesigned temperature to form barium hexaferrite powder. Water, due to its ease of acquirement and non-toxicity, is usually used as a solvent to dissolve the metallic salts. The precipitating agent commonly used is ammonia (NH₄OH) or caustic soda (NaOH) since hydroxide ions easily attack cations to form metallic hydroxides, and most of metallic hydroxides have low solubility in water. However, the solubility of barium hydroxide in water has a finite value though iron (III) hydroxide is insoluble in water. To overcome this problem and ensure the precipitates containing the required amounts of Fe³⁺ and Ba²⁺, the aqueous solution of metallic salts containing Fe³⁺/Ba²⁺ molar ratios less than 12 (a stoichiometric ratio of

* Tel.: +886226219473.

E-mail address: hfyu@mail.tku.edu.tw

$\text{Fe}^{3+}/\text{Ba}^{2+}$ to form $\text{BaFe}_{12}\text{O}_{19}$) is commonly adopted to prepare barium hexaferrites of high quality by coprecipitation [26–30].

In this study, a facile acetone-aided coprecipitation process was proposed to produce crystalline barium hexaferrite particles with high magnetic properties from an aqueous solution containing $\text{Fe}^{3+}/\text{Ba}^{2+}$ molar ratio of 12. Acetone was added in the precipitation liquid medium to adjust solubility of the derived metallic hydroxides during precipitation. Effects of the amount of acetone additions and the calcination temperature on characteristics and magnetic properties of the derived $\text{BaFe}_{12}\text{O}_{19}$ particles were investigated.

2. Experimental detail

2.1. Sample preparation

$\text{BaFe}_{12}\text{O}_{19}$ particles were synthesized using an acetone-aided coprecipitation method. Before reaction, two solutions (Soln-A and Soln-B) were prepared. Soln-A was formed by dissolving $\text{Fe}(\text{NO}_3)_3 \cdot 9\text{H}_2\text{O}$ (99% purity, Showa) and $\text{Ba}(\text{NO}_3)_2$ (99% purity, Showa), in a stoichiometric ratio to form $\text{BaFe}_{12}\text{O}_{19}$, in distilled water. The total metallic concentration of Soln-A was controlled at 0.85 M. Soln-B, acting as precipitation liquid medium, was a solution composed of distilled H_2O , acetone ($\text{CH}_3(\text{CO})\text{CH}_3$; 99.7%, Echo) and ammonia solution ($\text{NH}_4\text{OH}_{(\text{aq})}$; 29 wt%, Fisher) with volumetric ratio of $\text{H}_2\text{O}:\text{CH}_3(\text{CO})\text{CH}_3:\text{NH}_4\text{OH}_{(\text{aq})}=x:y:250$. Soln-A of 110 mL was then slowly added to the stirred Soln-B of 690 mL to undergo coprecipitation reaction at 20 °C for 2 h. Table 1 shows the various compositions of reaction system and the corresponding specimen codes. The amount of acetone in Soln-B was varied from 0 to 64 vol%. After reaction, the pH of the liquid system was 10.8 ± 0.1 for all the cases. The resultant suspension was centrifugally filtered. The collected wet cake was frozen at -45 °C and then dried in vacuum using a shelf type freeze dryer (FD12-2S-6P, Kingmech, Taiwan). The dried precipitates so obtained were calcined, in air, at different temperatures for 5 h or 48 h.

2.2. Characterization

Thermal behavior of the dried precipitates was investigated using a thermal analyzer STA 499 F3 (Netzsch, Germany), which is capable of performing thermogravimetric analysis (TG) and differential scanning calorimetry (DSC) simultaneously for the same sample. The organic or inorganic functional groups that existed in the specimens were detected using an infrared spectrometer (IR; Magna-IR spectrometer 550, Nicolet, Madison, WI, USA). The crystalline phases and crystal structure existing in the specimen were examined by X-ray diffraction analysis (XRD; D8A, Bruker, Germany). The X-ray source was $\text{Cu-K}\alpha$ radiation ($\lambda=1.54056 \text{ \AA}$), powered at 40 kV and 40 mA, and XRD data were collected from

25 to 45° (2θ) with a step size of 0.04° and a count time of 3 s. Based on the integrated peak intensities of the corresponding XRD patterns, mass ratios of different crystalline phases existing in the specimen were also estimated using a DIFFRAC^{plus} EVA software (Bruker, Germany). The molar ratio of Fe to Ba element existing in the specimens was measured using energy-dispersive X-ray spectroscopy (EDS; Bruker, Germany). Morphologies of the particles were observed using scanning electron microscopy (SEM; LEO 1530, Carl Zeiss, USA). The magnetic characteristics of some selected specimens were measured at room temperature using a superconducting quantum interference device magnetometer (SQUID; MPMS 7, Quantum Design, USA).

3. Results and discussion

3.1. Thermal behavior and phase development

By varying the amounts of acetone added in the coprecipitation procedure, five different dried precipitates (named A00, A16, A32, A48 and A64; refer to Table 1 for their exact contents) were obtained. Fig. 1 shows TG and DSC curves of these five different precipitates. For the dried precipitate obtained without any acetone addition (i.e., A00), two endothermic and two exothermic changes were detected during the course of heating. The first endothermic change at temperatures ranging from 45 °C to 150 °C was due to evaporation of the adsorbed water/acetone. A00 experienced the first exothermic change at 175–270 °C, which accompanied about 7.9% loss in weight. At 290–480 °C, the second endothermic change took place in the specimen, resulting in another 5.4% weight loss. Between 575 °C and 845 °C, the second exothermic change occurred and caused a slight decrease in weight (ca. 1.6 wt%). After adding acetone to the precipitation liquid medium, the weight loss of the specimen during heating

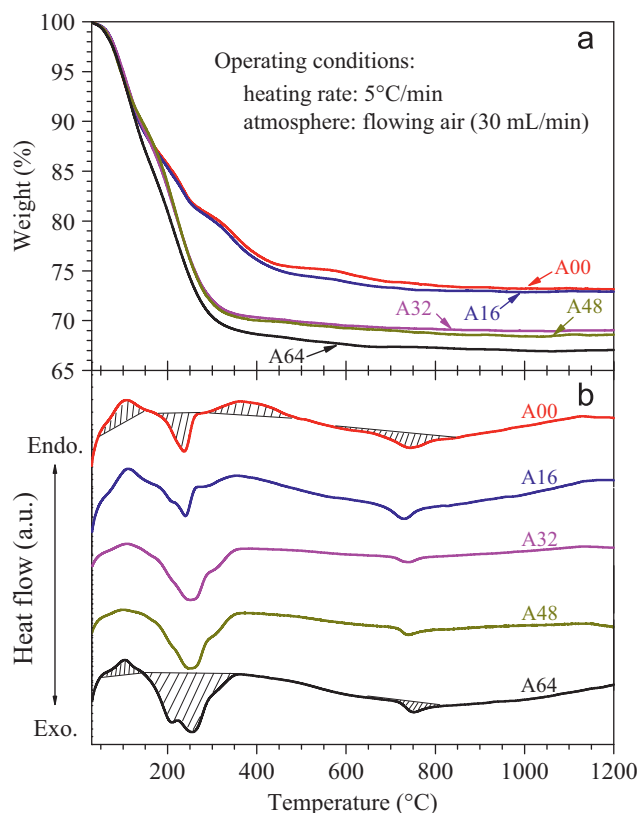


Fig. 1. (a) TG and (b) DSC curves of the dried precipitates.

Table 1
Compositions of the reaction system to prepare barium ferrite powder.

Specimen code	Soln-A ^a (mL)	Soln-B			
		Distilled H ₂ O (x, mL)	Acetone (y, mL)	NH ₄ OH _(aq) ^b (mL)	Percentage of acetone (vol%)
A00	110	440	0	250	0
A16	110	330	110	250	16
A32	110	220	220	250	32
A48	110	110	330	250	48
A64	110	0	440	250	64

^a Aqueous solution of ferric nitrate and barium nitrate, in a stoichiometric ratio to form $\text{BaFe}_{12}\text{O}_{19}$, with total metallic ions concentration of 0.85 M.

^b 29 wt% $\text{NH}_4\text{OH}_{(\text{aq})}$.

increased with increasing amount of the acetone additions. In the DSC curves, the addition of acetone caused the downward peak right after the first upward peak to become broader and to start splitting up to form a bimodal peak and the second upward peak to gradually vanish. In A64, a bimodal DSC peak, including at least two major exothermic reactions, was detected at temperatures between 145 °C and 360 °C, resulting in about 18.6% weight loss. Unlike A00, there was no endothermic change coming after the first exothermic change in A64. At 650–810 °C, the exothermic change occurring in A64 did not result in any conspicuous weight loss of the specimen. To recognize effects of these exothermic and endothermic changes on compositions of the specimen, A00 and A64 were heated, with a heating rate of 5 °C/min and in air, up to 300 °C, 600 °C and 700 °C without thermal soaking. The precipitates and the heated particles of A00 and A64 were IR-analyzed.

Fig. 2(a) shows IR spectra of the dried and heated A00 powders. For the dried A00, the IR bands for metallic hydroxo-complexes (i.e., the broad characteristic bands at 3432 and 427 cm⁻¹ [31]) were detected. The absorption band at 3130 cm⁻¹ was the characteristic band for NH₄⁺ and the band at 1623 cm⁻¹ indicated the existence of hydroxyl functional group (–OH). The strong absorption band at 1384 cm⁻¹ and the tiny band at 839 cm⁻¹ were ascribed to the presence of NO₃⁻ (a very strong band at 1520–1280 cm⁻¹) and CO₃²⁻ (a very strong band at 1530–1320 cm⁻¹ and a medium band at 890–800 cm⁻¹) [31]. Only the IR absorption bands of CO₃²⁻ were

detected in the A00 at 300 °C and these bands disappeared at 600 °C. The characteristic bands for BaFe₁₂O₁₉ [21,22] were detected in IR spectrum of the A00 at 700 °C. Accordingly, it was suggested that the solid precipitates obtained without acetone addition were mainly composed of hydroxo-complexes of iron and barium, ammonium nitrate (NH₄NO₃) and BaCO₃. The formation of BaCO₃ should be due to the reaction between the precipitated Ba(OH)₂ and the dissolved CO₂ in the precipitation liquid medium. By heating the dried A00 in air, NH₄NO₃ oxidized at the temperatures ranging from 175 °C to 270 °C (see Fig. 1(b)) and the evolved heat accelerated the decomposition of the hydroxo-complexes to form the oxides. The differences in IR spectra of A00 between 300 °C and 600 °C showed that the endothermic change, which accompanied with about 5.4 wt% loss, observed at 290–480 °C in the DSC curve for A00, removes BaCO₃, probably via the carbonate decomposition and/or the reaction between BaCO₃ and Fe₂O₃ existing in the specimen to form oxides. The appearance of IR characteristic bands for BaFe₁₂O₁₉ in the A00 at 700 °C suggested that the exothermic change that occurred at 575–845 °C in the A00 was mainly due to the crystallization of barium hexaferrites.

Fig. 2(b) is the IR spectra for the dried and heated A64. While the dried A64 had its IR spectrum similar to the dried A00, the IR spectrum of the A64 at 300 °C was much like the one for the A00 at 600 °C. At 700 °C, A64 converted to BaFe₁₂O₁₉. As discussed previously, the A64 should experience at least two exothermic reactions at temperatures between 145 °C and 360 °C (see the DSC curve for A64 in Fig. 1(b)). In addition to the oxidation of NH₄NO₃, what caused the other exothermic reaction? A test was conducted by heating the dried A64 at 210 °C, without thermal soaking, and IR-analyzing the specimen so obtained. However, the resultant IR spectrum showed no difference from that at 300 °C, implying that the heat evolved from the first exothermic reaction would immediately trigger the second exothermic reaction and would lead to a difficulty in isolating these reactions. In spite of this unresolved situation, IR analysis and thermal analysis (Fig. 1) indicated that increasing the added amounts of acetone in the precipitation liquid medium can decrease the formation of BaCO₃. Heating the dried A64 at temperatures above 300 °C can yield particles without any BaCO₃.

Fig. 3 gives XRD patterns of the A00 and A64 calcined at different temperatures for 5 h or 48 h. In Fig. 3(a), it can be found that the A00 calcined at 650 °C for 5 h was composed of hematite (α-Fe₂O₃; PDF #89-0599) and a trace of BaFe₁₂O₁₉ (PDF #43-0002). By extending the calcination time at 650 °C to 48 h, the crystallite size and amount of BaFe₁₂O₁₉ in the A00 were increased. Raising the calcination temperature could also promote the formation of BaFe₁₂O₁₉. However, α-Fe₂O₃ was still detected in the A00 at 1000 °C. Although the XRD results shown in Fig. 3(a) indicate that barium ferrite crystallites can be formed at temperature as low as 650 °C, the results also imply that A00 may not consist of stoichiometric amounts of Ba²⁺ and Fe³⁺ to form BaFe₁₂O₁₉, or may not have these ions uniformly distributed with each other. So, pure BaFe₁₂O₁₉ particles cannot be formed from the A00 precipitates, even after calcining the precipitates at 1000 °C. In A64 (see Fig. 3(b)), the changes in crystalline phases and crystallite sizes with calcination temperature and time were similar to those in the A00. Moreover, almost pure barium ferrite particles were produced by calcining A64 at 800 °C or above. Fig. 3(b) reveals that the acetone addition in the precipitation liquid medium (i.e., Soln-B) can lead to Ba²⁺ and Fe³⁺ in the solution co-precipitate, after reacting with NH₄OH, in a more uniform way and maintain the required ratio of Ba²⁺/Fe³⁺ in the precipitate to form BaFe₁₂O₁₉. It is to be noted that there were no distinguishable XRD peaks for Ba²⁺-contained compounds (e.g., BaCO₃, Ba(OH)₂, and BaO) found in all specimens, which should be due to low crystallinity or small quantities of these compounds.

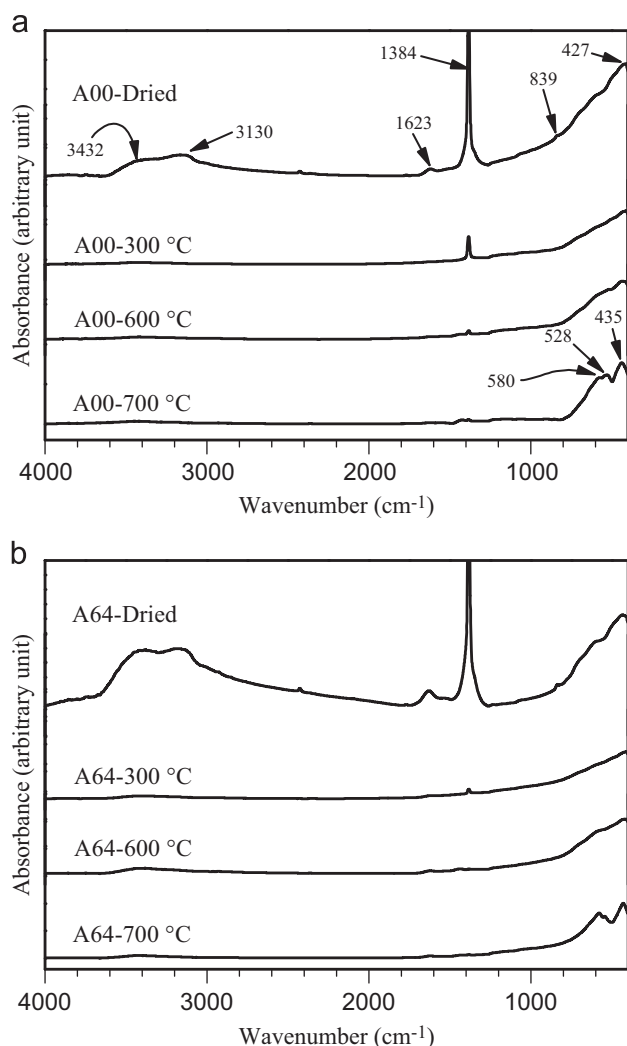


Fig. 2. IR spectra of (a) the A00 specimens and (b) the A64 specimens dried and calcined at 300 °C, 600 °C and 700 °C, without thermal soaking.

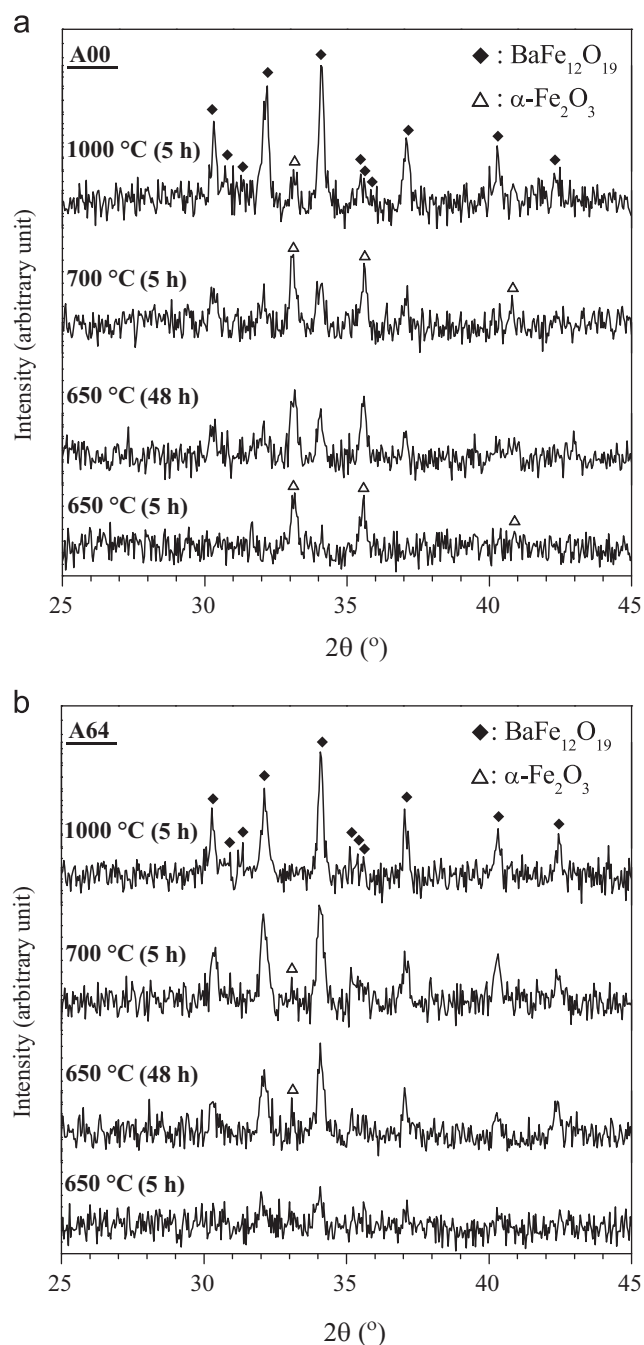


Fig. 3. XRD patterns for (a) A00 and (b) A64 calcined at different temperatures.

Effects of the amount of acetone additions on $\text{BaFe}_{12}\text{O}_{19}$ phase development were investigated by examining the amounts of $\alpha\text{-Fe}_2\text{O}_3$ and $\text{BaFe}_{12}\text{O}_{19}$ existing in the specimen. R is defined as mass ratio of $\alpha\text{-Fe}_2\text{O}_3$ to $\text{BaFe}_{12}\text{O}_{19}$ in the specimen; Fig. 4 shows how R varied with the amount of acetone added and the calcination temperature. At a fixed calcination temperature, R decreased apparently with increasing amount of the added acetone; for example, at 650 °C, R was 0.76 for A00 but reduced to only 0.14 for A64, and at 800 °C, R was 0.087 for A00 and was 0.016 for A64. Lower values in R mean that higher percentages of barium hexaferrite are formed. Accordingly, the addition of acetone in the precipitation liquid medium can effectively enhance the formation of $\text{BaFe}_{12}\text{O}_{19}$. On the other hand, regardless the amount of acetone added, R decreased rapidly with increasing calcination temperature until 800 °C and then slowly declined with further

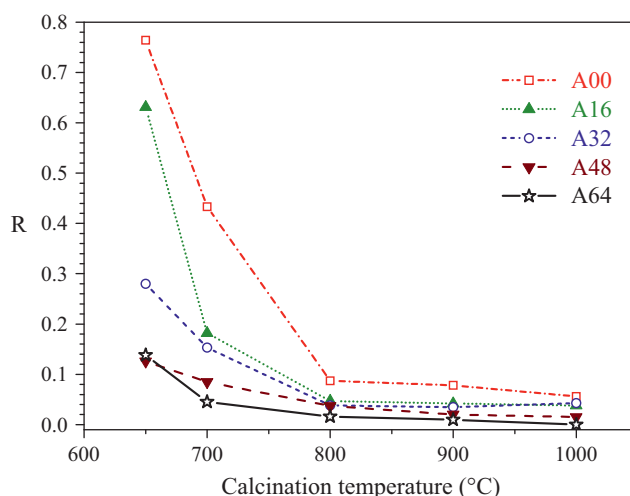


Fig. 4. $\text{Fe}_2\text{O}_3/\text{BaFe}_{12}\text{O}_{19}$ mass ratios (R) existing in the specimens.

increasing temperature. Although $\text{BaFe}_{12}\text{O}_{19}$ crystallites can be formed at 650 °C for the specimens prepared with or without acetone additions, a calcination temperature at 800 °C or higher is suggested to convert most of the precipitate to crystalline $\text{BaFe}_{12}\text{O}_{19}$ in short period of calcination time. It is to be noted that calcining A64 at 800 °C or above can produce pure $\text{BaFe}_{12}\text{O}_{19}$ particles.

To further confirm that the acetone addition in the precipitation liquid medium can force the barium ions to precipitate more completely and promote the formation of $\text{BaFe}_{12}\text{O}_{19}$, the specimens of A00, A32 and A64 were subjected to EDS analysis. It was found that the $\text{Fe}^{3+}/\text{Ba}^{2+}$ molar ratios were 14.8 for A00, 13.9 for A32 and 11.9 for A64, indicating that more acetone addition can lead the $\text{Fe}^{3+}/\text{Ba}^{2+}$ molar ratios in the precipitate more closer to the stoichiometric ratio required to form $\text{BaFe}_{12}\text{O}_{19}$. EDS analysis also explains the formation of pure $\text{BaFe}_{12}\text{O}_{19}$ for the A64 calcined at 800 °C or above.

Fig. 5 shows SEM images of some of the A64 and A00 specimens. Fig. 5(a) is a SEM image of the A64 calcined at 650 °C for 5 h, showing the existence of very small particles with some degree of particle agglomeration, as well as a tendency of the agglomerated particles to form plate-like structure. On extending the calcination time at 650 °C to 48 h, the particles grew in size and some plate-like hexagonal particles were observed, as shown in Fig. 5(b). XRD analysis on these two samples (see Fig. 3(b)) rationalized this morphology change, which was due to the increase of crystallinity of $\text{BaFe}_{12}\text{O}_{19}$ crystallites. Fig. 5(c) indicates that at 700 °C, more plate-like particles formed or started forming from the agglomerates of tiny spherical particles. The A64 at 1000 °C was composed of dispersive pure $\text{BaFe}_{12}\text{O}_{19}$ particles, evidenced by XRD analysis (Fig. 3(b)), with hexagonal plate-like structure (refer to Fig. 5(d)). For comparison, Fig. 5(e) and (f) gives the SEM images of the A00 at 700 °C and 1000 °C. Unlike the A64 at 700 °C, there were no distinct plate-like particles observed in the A00 at 700 °C. The hexagonal plate-like $\text{BaFe}_{12}\text{O}_{19}$ particles were formed in the A00 at 1000 °C but these plates were tightly compacted with each other, which may impede the development of magnetization of the particles.

3.2. Magnetic properties

Fig. 6(a) and (b) shows magnetic hysteresis loops of the A00 and A64 calcined at 700 °C, 800 °C and 1000 °C, respectively, and Table 2 summarizes magnetic properties of some other selected specimens. The A00 at 700 °C exhibited magnetization (measured at 50 kOe;

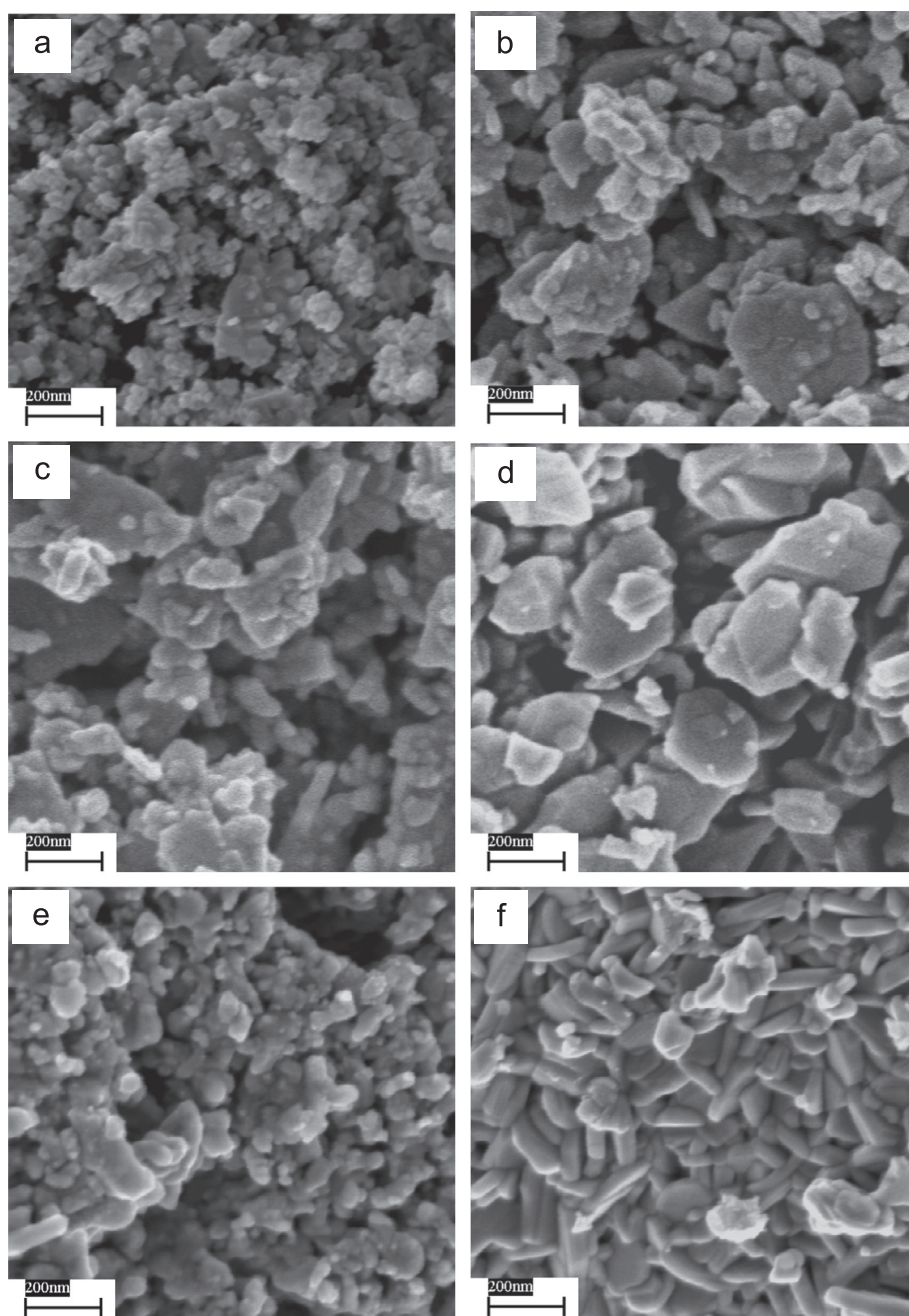


Fig. 5. SEM images of the A64 calcined at (a) 650 °C for 5 h, (b) 650 °C for 48 h, (c) 700 °C for 5 h and (d) 1000 °C for 5 h, as well as the A00 calcined at (e) 700 °C for 5 h and (f) 1000 °C for 5 h.

$M(50 \text{ kOe})$ of 28.3 emu/g, remanence magnetization (M_r) of 13.0 emu/g and coercivity (H_c) of 4.5 kOe. Further increasing the calcination temperature greatly increased the magnetic properties of A00. At 1000 °C, the A00 possessed $M(50 \text{ kOe})$ of 63.5 emu/g, M_r of 31.3 emu/g and H_c of 4.7 kOe. Adding acetone in the precipitation liquid medium, as discussed previously, can lead to precipitates with better quality (e.g., uniform distribution of Ba^{2+} and Fe^{3+} , molar ratio $\text{Fe}^{3+}/\text{Ba}^{2+} = 12$) and consequently plate-like hexagonal $\text{BaFe}_{12}\text{O}_{19}$ particles with high purity at lower calcination temperature. All of these effects due to acetone additions promoted magnetizations of the derived particles. For example, the A64 at 700 °C already possessed $M(50 \text{ kOe})$ of 57.4 emu/g and M_r of 26.3 emu/g. The A64 at 1000 °C exhibited $M(50 \text{ kOe})$ as high as 70.6 emu/g, which was 98% of the theoretical saturation magnetization of $\text{BaFe}_{12}\text{O}_{19}$ at room temperature (72 emu/g). The values of $M_r/M(50 \text{ kOe})$ for all of the calcined

specimens obtained in this study were equal or close to 0.5, indicating the formation of single magnetic domain size $\text{BaFe}_{12}\text{O}_{19}$ [32,33]. Fig. 7 gives changes of $M(50 \text{ kOe})$ of the specimens with amount of the acetone addition and calcination temperature. It clearly elucidates how the added acetone and the calcination temperature affect magnetization of the specimens. By combining the results shown in Figs. 4, 5 and 7, it can be concluded that adding acetone in the precipitation liquid medium can greatly promote formation of the crystalline $\text{BaFe}_{12}\text{O}_{19}$ at lower temperature and effectively enhance magnetization of the derived particles. On the other hand, raising the calcination temperature can also accelerate development of crystallite shape and magnetic characters of the barium hexaferrites. In this study, the barium hexaferrite powder obtained using a precipitation liquid medium of 64 vol% acetone and calcined at ≥ 900 °C gave the best performance in magnetization.

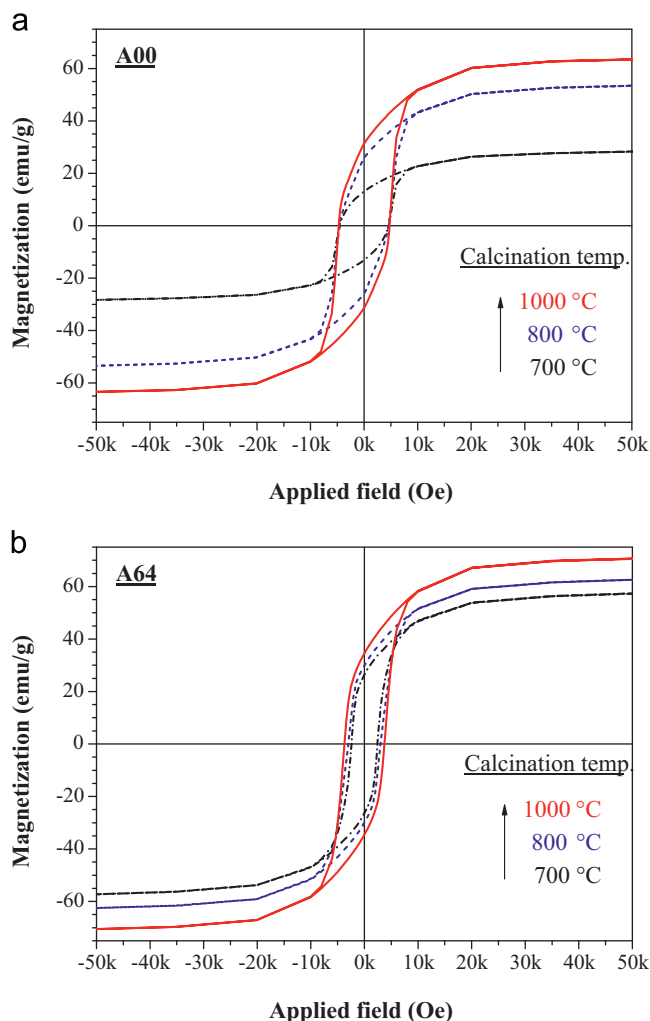


Fig. 6. Magnetic hysteresis loops for the specimens of the (a) A00 and (b) A64 calcined at 700, 800 and 1000 °C.

4. Conclusions

This study proposed a facile acetone-aided coprecipitation process to produce pure barium hexaferrite particles with high magnetization. Without acetone additions, $\text{BaFe}_{12}\text{O}_{19}$ crystallites may be formed by calcining the corresponding precipitate at 650 °C but pure crystalline $\text{BaFe}_{12}\text{O}_{19}$ particles cannot be obtained after calcining the precipitate even at 1000 °C for 5 h. Adding acetone to the precipitation liquid medium helped Ba^{2+} and Fe^{3+} in the solution to co-precipitate, after reacting with NH_4OH , in a more uniform way and to have the obtained precipitates containing the required $\text{Fe}^{3+}/\text{Ba}^{2+}$ molar ratio to form $\text{BaFe}_{12}\text{O}_{19}$. Increasing amounts of the added acetone can increase the ability of the precipitates to form crystalline $\text{BaFe}_{12}\text{O}_{19}$ at lower temperature and enhance magnetization of the derived particles. The precipitate obtained using the precipitation liquid medium of 64 vol% acetone (i.e., A64) was able to form pure $\text{BaFe}_{12}\text{O}_{19}$ particles at ≥ 800 °C. While the barium hexaferrite powder obtained without acetone additions and at 1000 °C had $M(50 \text{ kOe})$ of 63.5 emu/g, M_r of 31.3 emu/g and H_c of 4.7 kOe, the single magnetic domain size $\text{BaFe}_{12}\text{O}_{19}$ powder obtained using the precipitation liquid medium of 64 vol% acetone and calcining at 1000 °C possessed $M(50 \text{ kOe})$ of 70.6 emu/g, M_r of 34.4 emu/g and H_c of 3.7 kOe.

Table 2

Magnetic properties for some selected specimens.

Specimen	T (°C)	$M(50 \text{ kOe})$ (emu/g)	M_r (emu/g)	H_c (kOe)	$M_r/M(50 \text{ kOe})$
A00	700	28.3	13.0	4.5	0.46
	800	53.4	26.2	4.5	0.49
	900	57.5	28.6	4.7	0.50
	1000	63.5	31.3	4.7	0.49
A32	700	48	22.7	3.4	0.47
	800	–	–	–	–
	900	–	–	–	–
	1000	66.6	32.6	4.5	0.49
A48	700	52.9	24.4	2.3	0.46
	800	62.9	30.8	3.1	0.49
	900	68.5	34.0	3.3	0.50
	1000	68.5	33.6	3.6	0.49
A64	700	57.4	26.3	2.4	0.46
	800	62.6	30.2	3.1	0.48
	900	70.6	34.6	3.2	0.49
	1000	70.6	34.4	3.7	0.49

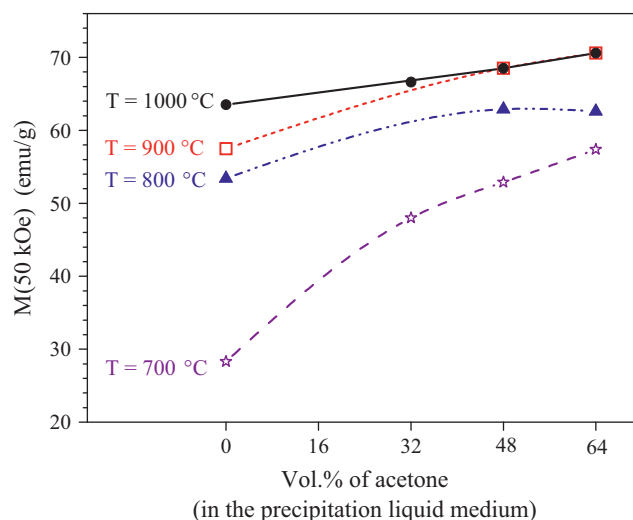


Fig. 7. Changes of $M(50 \text{ kOe})$ with amount of the added acetone and calcination temperature.

Acknowledgments

This research is financially supported by the National Science Council, Taiwan, under Grant no. NSC 100-2221-E-032-029. The assistances of Ms. Wei-Ying Wang and Ms. Wan-Ting Chu in this work are acknowledged.

References

- [1] T. Fujiwara, IEEE Transactions on Magnetics 21 (1985) 1480.
- [2] M. Imamura, Y. Ito, M. Fujiki, T. Hasegawa, H. Kubota, T. Fujiwara, IEEE Transactions on Magnetics 22 (1986) 1185.
- [3] K. Yamamori, T. Suzuki, T. Fujiwara, IEEE Transactions on Magnetics 22 (1986) 1188.
- [4] V. Pillai, P. Kumar, M.S. Multani, D.O. Shah, Colloids and Surfaces A: Physicochemical and Engineering Aspects 80 (1993) 69.
- [5] D. Lisjak, M. Drofenik, Journal of the European Ceramic Society 27 (2007) 4515.
- [6] M.M. Hessian, M. Radwan, M.M. Rashad, Journal of Analytical and Applied Pyrolysis 78 (2007) 282.
- [7] H.P. Steier, J. Requena, J.S. Moya, Journal of Materials Research 14 (1999) 3647.

- [8] H. Sozeri, *Journal of Alloys and Compounds* 486 (2009) 809.
- [9] B.T. Shirk, W.R. Buessem, *Journal of the American Ceramic Society* 53 (1970) 192.
- [10] E. Lucchini, S. Meriani, G. Slokar, *Journal of Materials Science* 18 (1983) 1331.
- [11] O. Kubo, T. Ido, H. Yokoyama, *IEEE Transactions on Magnetics* 18 (1982) 1122.
- [12] M. El-Hilo, H. Pfeiffer, K. O'Grady, W. Schuppel, E. Sinn, P. Gornert, M. Rosler, D. P.E. Dickson, R.W. Chantrell, *Journal of Magnetism and Magnetic Materials* 129 (1994) 339.
- [13] W.L. Wang, Z.W. Shih, C.H. Lin, *Journal of Crystal Growth* 130 (1993) 153.
- [14] X. Liu, J. Wang, L.M. Gan, S.C. Ng, *Journal of Magnetism and Magnetic Materials* 195 (1999) 452.
- [15] D. Mishra, S. Anand, R.K. Panda, R.P. Das, *Materials Chemistry and Physics* 86 (2004) 132.
- [16] T. Yamauchi, Y. Tsukahara, T. Sakata, H. Mori, T. Chikata, S. Katoh, Y. Wada, *Journal of Magnetism and Magnetic Materials* 321 (2009) 8.
- [17] Y. Liu, M.G.B. Drew, J. Wang, M. Zhang, Y. Liu, *Journal of Magnetism and Magnetic Materials* 322 (2010) 366.
- [18] L. Tai, P.A. Lessing, *Journal of Materials Research* 7 (1992) 502.
- [19] V.K. Sankaranarayanan, D.C. Khan, *Journal of Magnetism and Magnetic Materials* 153 (1996) 337.
- [20] D. Bahadur, W. Fischer, M.V. Rane, *Materials Science and Engineering A* 252 (1998) 109.
- [21] H.F. Yu, K.C. Huang, *Journal of Magnetism and Magnetic Materials* 260 (2003) 455.
- [22] H.F. Yu, P.C. Liu, *Journal of Alloys and Compounds* 416 (2006) 222.
- [23] S.E. Jacobo, L. Civalé, C. Domingo-Pascual, R. Rodrigues-Clements, M.A. Blesa, *Journal of Materials Science* 32 (1997) 1025.
- [24] O. Carp, R. Barjega, E. Segal, M. Brezeanu, *Thermochimica Acta* 318 (1998) 57.
- [25] T. Ogasawara, M.A.S. Oliveira, *Journal of Magnetism and Magnetic Materials* 217 (2000) 147.
- [26] S.R. Janasi, D. Rodrigues, F.J.G. Landgraf, M. Emura, *IEEE Transactions on Magnetics* 36 (2000) 3327.
- [27] W.K. Ng, J. Ding, Y.Y. Chow, S. Wang, Y. Shi, *Journal of Materials Research* 15 (2000) 2151.
- [28] M. Montazeri-Pour, A. Ataie, *International Journal of Modern Physics B* 22 (2008) 3144.
- [29] M. Montazeri-Pour, A. Ataie, *Journal of Materials Science and Technology* 25 (2009) 465.
- [30] M.M. Rashad, I.A. Ibrahim, *Journal of Magnetism and Magnetic Materials* 323 (2011) 2158.
- [31] G. Socrates, *Infrared and Raman Characteristic Group Frequencies—Tables and Charts*, 3rd ed., Wiley, New York, 2001.
- [32] E.C. Stoner, E.P. Wohlfarth, *Philosophical Transactions of the Royal Society A* 240 (1946–1948) 600.
- [33] P. Kerschl, R. Grössinger, C. Kussbach, R. Sato-Turtelli, K.H. Müller, L. Schultz, *Journal of Magnetism and Magnetic Materials* 242–245 (2002) 1468.